Research Square

Preprints are preliminary reports that have not undergone peer review.
They should not be considered conclusive, used to inform clinical practice,
or referenced by the media as validated information.

Temperature as a Lorentz four-vector:a standard-free test from stochastic fields

Ira Wolfson

wolfsoni@braude.ac.il

Braude College of Engineering Karmiel

Article

Keywords:

Posted Date: November 12th, 2026

DOI: https://doi.org/10.21203/rs.3.rs-11529534/v1

License: This work is licensed under a Creative Commons Attribution 4.0 International License.
Read Full License

Additional Declarations: No competing interests reported.

Temperature as a Lorentz four-vector: a standard-free test from stochastic fields

Ira Wolfson
Department of Electrical and Electronic Engineering,
Braude Academic College of Engineering, Karmiel 2161002, Israel
wolfsoni@braude.ac.il

Abstract

Planck said a moving body looks cooler, Ott said hotter, and Landsberg said unchanged. The controversy, open since 1908, was settled theoretically by recognizing that relativistic equilibrium is carried by the inverse-temperature four-vector $\beta^\mu = u^\mu/(k_B T_0)$. That resolution has never been tested, because no experiment has measured the thermal state of a moving medium at several angles at once. We prove that both components of β^μ can be reconstructed from a single passive observable, the electromagnetic fluctuation correlations of a drifting medium, with no active probe, no spectral lines and no absolute radiometric calibration. A dimensionless electric-magnetic cross-spectral ratio fixes the drift velocity through the Lorentz mixing of the field-strength tensor; the angle-resolved noise power, governed by the covariant fluctuation-dissipation theorem, fixes the rest-frame temperature. The reconstructed rest-frame temperature is flat in angle if and only if the thermal state transforms as β^μ, so angular flatness is an operational, standard-free test of the Lorentz transformation law of temperature. Monte-Carlo simulations parameterized to the HIGGINS dual-100 TW laser-plasma facility show that the test is realizable for Lorentz factors γ from 1.05 to 10, with sub-percent recovery of the rest-frame temperature for $\gamma \leq 2$. A century-old argument becomes a measurement.

1 Introduction

Planck said a moving body appears cooler (T_0/γ), Ott said hotter ($T_0\gamma$), and Landsberg said unchanged (the invariant T_0) [1, 2, 3]. The Planck–Ott–Landsberg controversy was resolved theoretically by recognizing that temperature is one component of the inverse-temperature four-vector $\beta^\mu = u^\mu/(k_B T_0)$ [4, 5, 6, 7], though the question continues to attract debate [8, 9]. This covariant structure, originating in the nonequilibrium statistical operator formalism of Zubarev [10] and placed on rigorous footing by van Kampen [4] and Israel [5], now underpins relativistic dissipative hydrodynamics and the Kubo–Martin–Schwinger condition in thermal field theory [11, 12, 13].

That resolution has never been tested. It rests entirely on theoretical arguments and thermodynamic consistency: no experiment has ever measured the thermal state of a relativistic medium at multiple observation angles and checked that the results are consistent with four-vector transformation. The obstruction is observational. Reconstructing a four-vector requires the rest-frame temperature T_0 and the four-velocity u^μ to be pinned down together, at more than one angle, from the same physical state; existing thermometry supplies them separately and at a single sightline.

Every current technique infers T_0 and u^μ from independent observables, and each carries a structural limitation that blocks model-independent access to the covariant state. Heavy-ion blast-wave fits [14] read temperature from invariant-mass spectra and velocity from collective flow (v_1, v_2), so the resulting β^μ is a hydrodynamic fit parameter, not an observable. Thomson scattering [15]

gives an accurate electron temperature but needs an external laser probe and an independent Doppler measurement for the flow. Spectral radiometry [16, 17] requires absolutely calibrated detectors and a separately supplied drift velocity. Astrophysical sources [18] deliver a single line of sight only, making the angle-resolved measurement a four-vector demands geometrically impossible. (Angle-resolved synchrotron radiation, while relativistic, is coherent single-particle emission, not equilibrium thermal fluctuations; it tests classical electrodynamics, not the statistical mechanics of a thermal ensemble.)

We prove that both components of β^μ can be read out of one passive observable (the electromagnetic fluctuation correlations emitted by a drifting medium), and that the reconstruction carries its own falsifiable signature of the transformation law: the reconstructed rest-frame temperature is flat in angle if and only if the thermal state transforms as β^μ (Corollary 2). The laser-plasma numerics, the implementation and the systematics show that the test is realizable (§2.7 and Methods).

2 Results

2.1 Definitions and borrowed foundations

We work in flat spacetime with metric signature $(+,-,-,-)$ and set $c = 1$ except where a factor of c aids readability. The medium is in local thermodynamic equilibrium in its rest frame and drifts with constant velocity β along $\hat{z}$ relative to the laboratory; $\gamma = (1-\beta^2)^{-1/2}$.

Definition 1 (Inverse-temperature four-vector)**.** $\beta^\mu = u^\mu/(k_B T_0)$, with u^μ the medium four-velocity and T_0 its rest-frame temperature [10, 4, 5]. This is the target of reconstruction.

Definition 2 (E–B cross-spectral ratio)**.** $R \equiv \langle \delta E'_y\, \delta B'^{*}_x \rangle / \langle |\delta E'_y|^2 \rangle$, formed from the laboratory-frame transverse field fluctuations, with E and cB expressed in commensurate units so that R is dimensionless.

Definition 3 (Doppler factor)**.** $D(\theta) = \gamma(1-\beta\cos\theta)$, relating rest-frame and laboratory frequencies by $\omega = D\,\omega'$ for radiation emitted at laboratory angle θ to the drift axis.

The three theorems draw on three standard results, stated here without proof and used as quoted.

B1 (Lorentz boost of the field-strength tensor). Under a boost $\beta\hat{z}$, the transverse field components mix as

$$E'_y = \gamma(E_y + vB_x), \qquad B'_x = \gamma\big(B_x + \tfrac{v}{c^2}E_y\big)\,, \tag{1}$$

obtained from $F'^{\mu\nu} = \Lambda^\mu{}_\alpha \Lambda^\nu{}_\beta F^{\alpha\beta}$ applied to the $(0,2)$ and $(1,3)$ components.

B2 (Covariant fluctuation–dissipation theorem). In equilibrium the symmetric and retarded current–current correlators satisfy

$$\Pi^{\mu\nu}_S(p) = \coth\big(\tfrac{1}{2}\beta\cdot p\big)\, 2\,\mathrm{Im}\,\Pi^{\mu\nu}_R(p), \qquad \beta\cdot p = \beta^\mu p_\mu, \tag{2}$$

with $\beta\cdot p$ Lorentz-invariant; the coth is the thermal mode occupation and the relation follows from the KMS condition [19, 20, 12, 13].

B3 (Lorentz invariance of I_ν/ν^3). The specific intensity obeys $I'_{\nu'}/\nu'^3 = I_\nu/\nu^3$, a restatement of the invariance of the photon phase-space occupation number [17].

2.2 Velocity from the cross-spectral ratio

Theorem 1 (Velocity from the E–B cross-spectral ratio)**.** *For a medium with isotropic rest-frame field fluctuations drifting at velocity β, the cross-spectral ratio of Definition 2 is*

$$R = \frac{2\beta}{1+\beta^2}, \qquad \textit{invertible to} \qquad \beta = \frac{1-\sqrt{1-R^2}}{R}. \tag{3}$$

Proof. (i) Rest-frame isotropy gives $\langle \delta E_y \, \delta B_x^* \rangle = 0$. (ii) Apply B1. The laboratory cross-spectral density is

$$\langle \delta E_y' \, \delta B_x'^* \rangle = \gamma^2 \left[\tfrac{v}{c^2} \langle |E_y|^2 \rangle + v \langle |B_x|^2 \rangle \right],$$

the two $\langle E_y B_x^* \rangle$ cross terms vanishing by (i). (iii) Far-field detection in vacuum imposes Poynting equipartition $\langle |E|^2 \rangle = c^2 \langle |B|^2 \rangle$, i.e. $\langle |B_x|^2 \rangle = \langle |E_y|^2 \rangle / c^2$, so the numerator reduces to $\gamma^2 (2v/c^2) \langle |E_y|^2 \rangle = \gamma^2 \, 2\beta \, \langle |E_y|^2 \rangle$ in commensurate units. (iv) The denominator is $\langle |\delta E_y'|^2 \rangle = \gamma^2 (\langle |E_y|^2 \rangle + v^2 \langle |B_x|^2 \rangle) = \gamma^2 (1+\beta^2) \langle |E_y|^2 \rangle$. (v) The ratio is $R = 2\beta/(1+\beta^2)$; the quadratic $\beta^2 R - 2\beta + R = 0$ inverts to $\beta = (1-\sqrt{1-R^2})/R$, taking the physical root $\beta \in [0, 1)$. □

Corollary 1 (The velocity observable is thermal-model-independent)**.** *β is recovered for* any *medium with isotropic rest-frame fluctuations, whether or not the distribution is Jüttner [21] or in equilibrium.*

Proof. The proof of Theorem 1 invokes only rest-frame isotropy ($\langle \delta E_y \, \delta B_x^* \rangle = 0$) and the Lorentz structure of $F^{\mu\nu}$ (B1). It nowhere uses the distribution function; hence it holds for any isotropic rest-frame ensemble. □

2.3 Temperature from angle-resolved noise

Theorem 2 (Angular thermal power spectrum of a drifting equilibrium medium)**.** *The laboratory power spectral density of the thermal field fluctuations at angle θ is*

$$S(\omega', \theta) \propto \frac{T_0}{D(\theta)} \, \sigma(D(\theta) \, \omega'), \qquad D(\theta) = \gamma(1 - \beta \cos\theta), \tag{4}$$

where σ is the medium response function; the effective laboratory temperature is T_0/D.

Proof. (i) In the classical limit $\hbar\omega \ll k_B T_0$ the coth of B2 linearizes, $\coth(x) \to 1/x$, giving the rest-frame PSD $S_{\text{rest}}(\omega) \propto T_0 \, \sigma(\omega)$. (ii) Transform to the laboratory: relativistic beaming (B3) fixes the intensity scaling, the density-of-states projection supplies the remaining powers of D, and $\omega = D\omega'$ carries the argument. (iii) Collecting the powers of D yields $S(\omega', \theta) \propto (T_0/D) \, \sigma(D\omega')$. The exhaustive D-power bookkeeping (the beaming factor D^{-3} against the prefactor D^{+2}, netting D^{-1}) is carried out in Methods (§4.1). □

2.4 Reconstruction of the four-vector

Theorem 3 (Operational reconstruction of β^μ from a single passive observable)**.** *From one stochastic-field ensemble, the inverse-temperature four-vector $\beta^\mu = u^\mu/(k_B T_0)$ is reconstructed with no active probe, no spectral lines, and no absolute radiometric calibration.*

Proof. (i) β follows from R by Theorem 1, requiring only a stable relative E/B channel gain. (ii) With β fixed, Theorem 2 gives the laboratory temperature $T_{\text{lab}}(\theta) = T_0/D(\theta)$; a rest-frame calibration spectrum W_{rest} cancels the absolute amplitude in the ratio $W_{\text{lab}}/W_{\text{rest}}$, leaving $T_0(\theta) = D(\theta) \, T_{\text{lab}}(\theta)$ at each angle and requiring only knowledge of the response $\sigma(\omega)$. (iii) The direction and magnitude of β give u^μ, and (ii) gives T_0; together they assemble β^μ, every input drawn from the same passive field ensemble. □

2.5 The four-vector transformation test

Through its angular structure, the reconstruction of Theorem 3 is also a falsifiable test of the transformation law itself.

Corollary 2 (Angular flatness is a direct test of the four-vector transformation of temperature)**.** *The reconstructed rest-frame temperature*

$$T_0^{(\mathrm{rec})}(\theta) = D(\theta)\, T_{\mathrm{lab}}(\theta) \tag{5}$$

is independent of angle if and only if *the thermal state transforms as the four-vector β^μ. Angular flatness is therefore an operational, standard-free test of the Lorentz transformation law of temperature.*

Proof. ($\Rightarrow$) If the thermal state is the four-vector β^μ, Theorem 2 gives $T_{\mathrm{lab}}(\theta) = T_0/D(\theta)$ exactly, so $D(\theta)\, T_{\mathrm{lab}}(\theta) = T_0$ for every θ: the reconstruction is flat. ($\Leftarrow$) Planck's T_0/γ, Ott's $T_0\gamma$ and Landsberg's invariant T_0 are scalar prescriptions: each assigns the moving medium a single laboratory temperature, independent of θ, so $D(\theta)\, T_{\mathrm{lab}} \propto D(\theta)$, which varies with θ for any $\beta > 0$. More generally, $D(\theta)\, T_{\mathrm{lab}}(\theta)$ is constant only if $T_{\mathrm{lab}}(\theta) \propto 1/D(\theta)$, the four-vector prediction of Theorem 2. Flatness measured across independent angles selects the four-vector law and falsifies the alternatives, using no external temperature or velocity standard. □

The controversy has been settled on paper for a century; Corollary 2 makes it a measurement. A single drifting equilibrium medium, observed passively at several angles, either returns an angle-flat $T_0^{(\mathrm{rec})}$ (confirming four-vector transformation) or it does not, and the residual angular slope discriminates directly between the Planck, Ott, and Landsberg alternatives. No universal form of the transformation law exists in general [22], which makes a direct empirical selection the more valuable.

2.6 Relation to thermal emission

The equivalence to Doppler-shifted thermal emission is the method's physical basis. In equilibrium, Kirchhoff's law ties emission to absorption, and the Lorentz invariance of I_ν/ν^3 (B3) gives boosted thermal radiation the same angular factor $T_0/[\gamma(1-\beta\cos\theta)]$ that appears in Theorem 2; at bottom the protocol is relativistic thermal radiometry. The relation is exactly that between Johnson–Nyquist noise thermometry and Planck's law: Johnson's 1928 measurement of voltage noise across a resistor [23, 24] was novel not because it revealed new radiation physics (Planck's law was long known) but because the observable (voltage variance), the required calibration (resistance, not an absolute radiometric standard), and the practical reach were different. The present protocol stands in the same relation to boosted blackbody radiometry, and differs from it in three operational respects. *(i) Observable*: the E–B cross-spectral ratio accesses the off-diagonal sector of the boosted $F^{\mu\nu}$, which intensity radiometry and Stokes polarimetry (both confined to $\langle E_i E_j^* \rangle$) cannot reach. *(ii) Calibration*: the velocity needs only relative E/B channel stability and the temperature only a rest-frame power ratio; neither needs an absolute radiometric standard. *(iii) Closure*: conventional radiometry of a moving source yields $T_0/D(\theta)$ but cannot separate T_0 from β, whereas the E–B ratio supplies β from the same field, closing the system and delivering β^μ from a single measurement.

2.7 Realizability

The theorems above stand on their own; what remains is whether the protocol they define can be built. It can. Monte-Carlo simulations parameterized to the HIGGINS dual-100 TW laser-plasma

facility [25] carry a synthetic equilibrium medium through the full reconstruction of Theorem 3 and the flatness test of Corollary 2, recovering the rest-frame temperature to sub-percent accuracy for Lorentz factors $\gamma \leq 2$ and to $\approx 6\%$ at $\gamma = 10$ (the degradation set by forward-beaming mode starvation, not by the method), with the velocity channel accurate across the range and the flatness test resolved cleanly for a signal-to-noise ratio $\gtrsim 10$ under dark-frame subtraction. The measurement needs only relative E–B channel calibration, knowledge of the medium response $\sigma(\omega)$, and local thermodynamic equilibrium. Passive fluctuation spectroscopy is already an established plasma diagnostic in the non-relativistic regime [26]; the present protocol extends the principle to relativistic media and to reconstruction of the full β^μ. The complete apparatus, algorithm, parameter set, systematics, and the simulated flatness test are given in Methods (§§4.1–4.2).

3 Discussion

The inverse-temperature four-vector has been the accepted description of relativistic equilibrium for half a century, yet it has lived entirely in theory: a quantity every relativistic hydrodynamics code assumes and no experiment has ever returned as a single measured object. What has been a consistency argument since 1908 becomes, in Corollary 2, an angle-flatness signature that an experiment can confirm or break.

In relativistic heavy-ion collisions, "temperature" is routinely extracted from particle spectra under the assumption that the thermal state transforms as a four-vector, an assumption built into the analysis framework rather than tested by it; a controlled laboratory confirmation (or falsification) of the four-vector law would supply the empirical baseline those analyses presently lack. In astrophysical settings such as gamma-ray bursts, the principle of reading thermal parameters from passive fluctuation statistics could inform single-sightline analyses once the multi-angle protocol is validated. The laboratory measurement is the first link in that chain.

4 Methods

4.1 Derivation of the laboratory-frame PSD

This section derives Eq. (4) from first principles, tracking all frequency-dependent prefactors through the Lorentz transformation. The textbook ingredients are Rybicki & Lightman [17] (radiative transfer and the invariance of I_ν/ν^3) and Kapusta & Gale [12] (finite-temperature field theory and the covariant FDT).

Starting from the rest-frame PSD with all prefactors, the classical limit $\coth(\hbar\omega/2k_BT_0) \to 2k_BT_0/\hbar\omega$ gives $S_{\rm rest}(\omega) \propto T_0\,\sigma(\omega)$. The Doppler relation $\omega = D\omega'$ with $D = \gamma(1-\beta\cos\theta)$ maps frequencies between frames. The invariance $I'_{\nu'}/\nu'^3 = I_\nu/\nu^3$ supplies a beaming factor D^{-3}; the density-of-states projection prefactor (from ω^2 in the electric-field spectral weight) supplies D^{+2}; their product with the frequency-argument substitution collects as

$$\underbrace{D^{-3}}_{\text{beaming}} \times \underbrace{D^{+2}}_{\omega^2\ \text{prefactor}} = D^{-1}, \tag{6}$$

so that

$$S(\omega',\theta) \propto \frac{T_0}{D}\,\sigma(D\omega') = \frac{T_0}{\gamma(1-\beta\cos\theta)}\,\sigma\big(\gamma\omega'(1-\beta\cos\theta)\big)\,, \tag{7}$$

which is Eq. (4). The single surviving power D^{-1} is the source of the T_0/D effective laboratory temperature and hence of the flatness test of Corollary 2. The D^{-3} beaming factor alone would

produce a strong angular modulation; the ω^2 density-of-states factor, sampling σ at the Doppler-shifted frequency, partially compensates it, leaving the net D^{-1}.

4.2 Experimental realization and numerical validation

This section specifies the complete measurement (simulation model, calibration, the simulated flatness test, robustness studies, hardware, systematics, algorithm, and parameters) in sufficient detail for independent reproduction, and establishes that the protocol is realizable with existing infrastructure.

4.2.1 Simulation model

The simulation generates an ensemble of $N_{\rm mode} = 4\times10^4$ thermal electromagnetic modes in the rest frame of the plasma, uniformly distributed in direction (isotropic) and frequency $\omega \in [0.1, 13.0]\,\omega_p$, where $\omega_p = (n_e e^2/\varepsilon_0 m_e)^{1/2} \approx 1.78\times10^{14}\,\mathrm{rad/s}$ ($f_p \approx 28\,\mathrm{THz}$). Mode amplitudes follow the classical FDT with a Drude conductivity $\sigma(\omega) = \nu/(\nu^2+\omega^2)$, collision frequency $\nu/\omega_p = 0.05$, and electron temperature $T_0 = 1\,\mathrm{keV}$ ($k_B T_0/\hbar\omega_p = 8512$, deep in the classical regime). All modes are boosted to the laboratory frame at velocity βc via Eq. (1) and relativistic aberration, and binned by a ring of 12 detector pixels spanning $\theta = 15^\circ$ to 165°.

4.2.2 Two-step calibration protocol

Step 1 (calibration) measures the plasma at rest ($\beta = 0$), giving an angular reference $W_{\rm rest}(\theta) \propto \sin\theta\, P_{E_y}(\theta, 0) \int \sigma\, d\omega$. Step 2 measures the boosted plasma,

$$W_{\rm lab}(\theta) \propto \frac{\sin\theta}{D^2(\theta)}\, P_{E_y}(\theta,\beta)\, T_0 \int \sigma(D\omega')\, d\omega', \tag{8}$$

with P_{E_y} the azimuth-averaged polarization projection. The ratio $W_{\rm lab}/W_{\rm rest}$ cancels the calibration-dependent amplitude; in the high-frequency regime $\int \sigma(D\omega')\,d\omega' / \int \sigma\, d\omega \;\to\; D^{-1}$, from which $T_{\rm lab}(\theta) = T_0/D(\theta)$ is extracted using $\beta_{\rm EB}$ from the E–B ratio.

4.2.3 The flatness test

Figure 1 is the four-vector transformation test carried out on the Monte-Carlo data at $\gamma = 1.5$, with the drift velocity $\beta_{\rm EB} = 0.746$ recovered from the E–B correlation (10,000 realizations, 4×10^4 modes each). Panel (a) is the raw angular thermometry: the reconstructed effective laboratory temperature (points) follows the four-vector prediction $T_{\rm lab}(\theta) = T_0/D(\theta)$ across the ring, sweeping a factor of $\sim$6, whereas a Lorentz-invariant temperature would give the flat dashed line. Panel (b) is the test proper: multiplying by $D(\theta)$ collapses the swept data to a flat $T_0^{(\rm rec)}(\theta) = T_0$ at 0.34% RMS across all 12 pixels, while any non-four-vector law leaves a residual angular slope $\propto D(\theta)$ (dashed). The same run recovers the angular profile to 0.34% RMS (Fig. 2) and the velocity to 0.1%; robustness of the flatness signature under injected rest-frame anisotropy is shown in Fig. 5(a).

4.2.4 Single-γ and multi-γ recovery

At $\gamma = 1.5$ the angular temperature profile is recovered to 0.34% RMS across all 12 pixels (Fig. 2), the forward and backward pixels spanning a factor of ~ 7 in apparent temperature, a direct manifestation of the Doppler factor in the covariant thermal state. Repeating the extraction for $\gamma \in \{1.05, 1.1, 1.2, 1.5, 2, 3, 5, 10\}$ (Fig. 3) recovers T_0 to sub-percent accuracy for $\gamma \le 2$, degrading

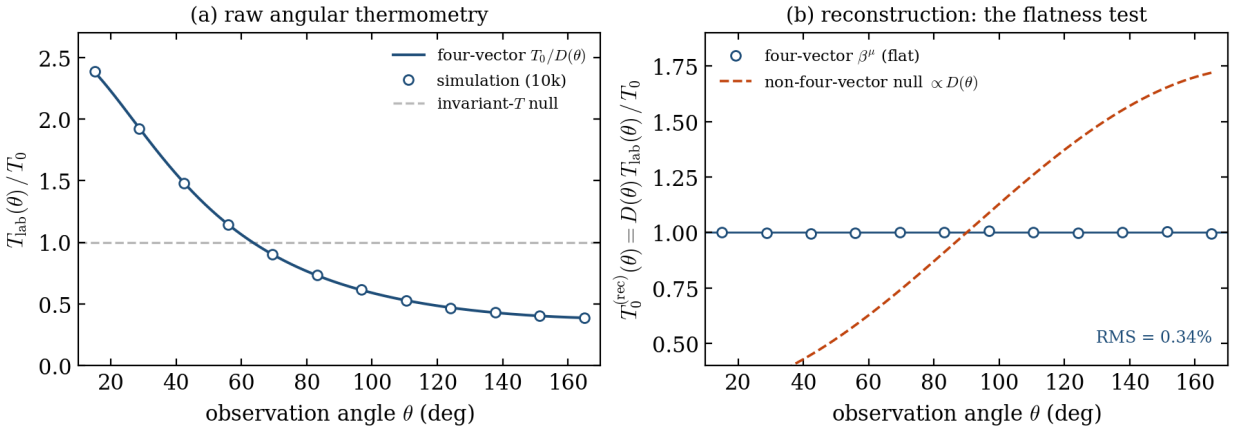


Figure 1: The four-vector transformation test (Corollary 2) on Monte-Carlo data at $\gamma = 1.5$, HIGGINS parameters, 10,000 realizations ($\beta_{\rm EB} = 0.7456$). (a) Raw angular thermometry: the reconstructed effective laboratory temperature (points) follows $T_0/D(\theta)$ (solid), sweeping a factor of ~ 6; the invariant-temperature null is flat (dashed grey). (b) Reconstruction: $T_0^{(\rm rec)}(\theta) = D(\theta)\,T_{\rm lab}(\theta)$ is flat to 0.34% RMS under the four-vector law (points on the solid line), whereas a competing law leaves a residual slope $\propto D(\theta)$ (dashed). Flatness across independent angles is the signature that selects the four-vector law.

to $\sim 2\%$ at $\gamma = 3$ and $\sim 6\%$ at $\gamma = 10$. The degradation is physical: relativistic beaming concentrates radiation into a narrow forward cone, starving backward-angle pixels of modes (831 modes per pixel at $\gamma = 1.05$ versus 223 at $\gamma = 10$).

4.2.5 Noise susceptibility

Additive detector noise is modeled as a flat power floor $P_{\rm noise} = \langle P_{\rm signal}\rangle/{\rm SNR}$ with exponential pixel-level fluctuations (Fig. 4). Without subtraction the floor biases T_0 upward by $\sim 100/{\rm SNR}\%$; with a separately measured dark frame subtracted, the bias is removed and the total recovery error stays below 10% for SNR $\gtrsim 10$ at $\gamma = 1.5$. These thresholds are within the reach of mid-infrared bolometer arrays at $\lambda \sim 10\,\mu$m.

4.2.6 Experimental implementation

The HIGGINS system [25] delivers two independently compressed 100 TW pulses (7 J split, 30 fs, 800 nm) onto a nitrogen supersonic gas jet; the electron population thermalizes on sub-picosecond timescales with $T_e \sim 1$ keV and $\omega_p \approx 28$ THz. The diagnostic requires a ring of ~ 12 mid-infrared detectors (MCT or pyroelectric bolometers at $\lambda \sim 10\,\mu$m) at $R \approx 50$ cm, spanning 15° to 165° relative to the drift direction, with ~ 3 cm apertures ($\Delta\theta \approx 3.4°$). The E–B cross-correlation is measured by dual-polarization detection or split-path pickup, as in microwave polarimetry [16]. At the 1 Hz repetition rate, ensemble averaging over $\sim 10^3$ shots takes ~ 15 minutes per γ setting.

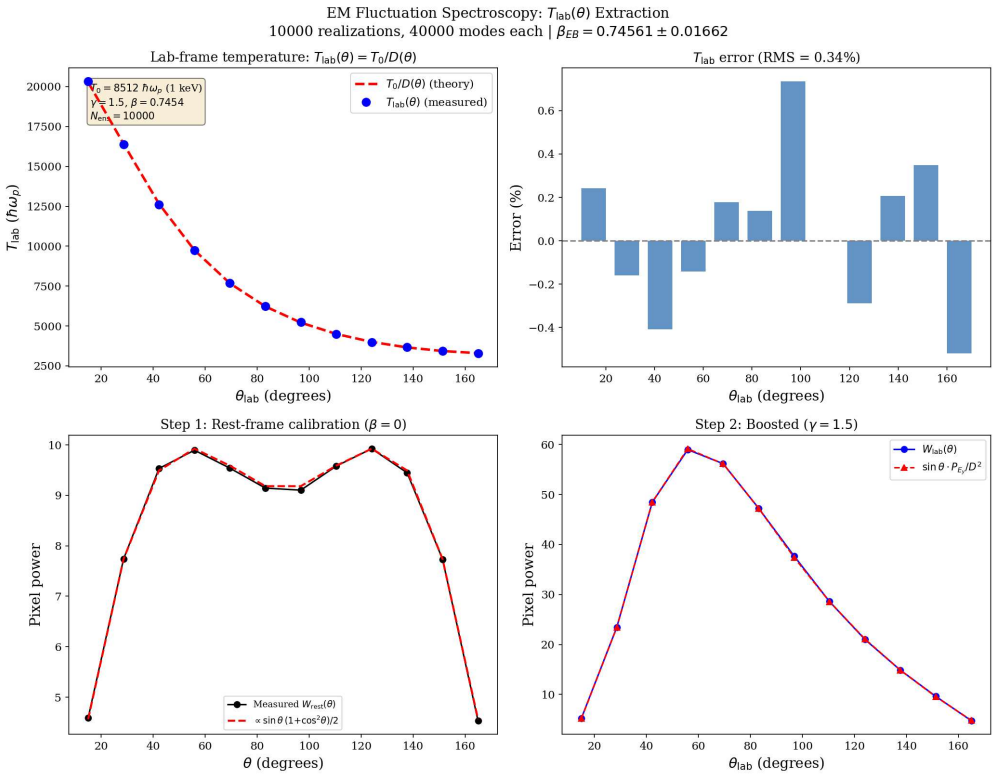


Figure 2: Single-γ angular thermometry at $\gamma = 1.5$; recovered $T_{\rm lab}(\theta)$ at 12 pixels agrees with $T_0/D(\theta)$ to 0.34% RMS.

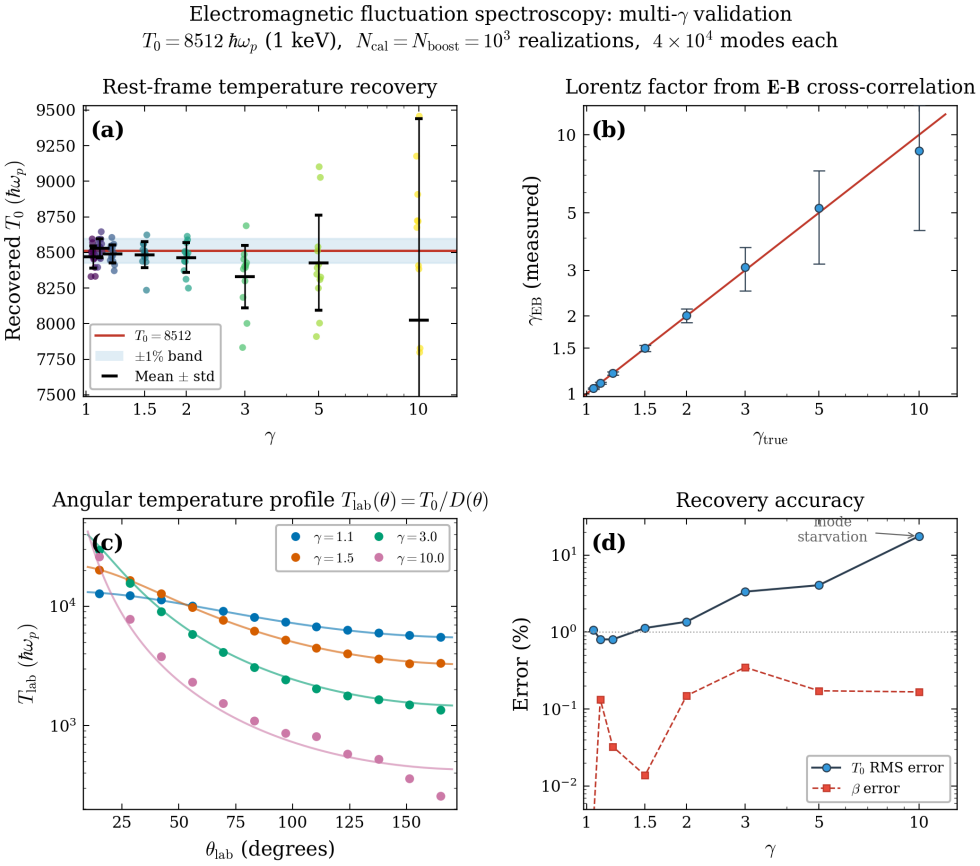


Figure 3: Multi-γ validation of T_0 recovery over $\gamma = 1.05$–10, with the Lorentz factor independently recovered from the E–B cross-correlation.

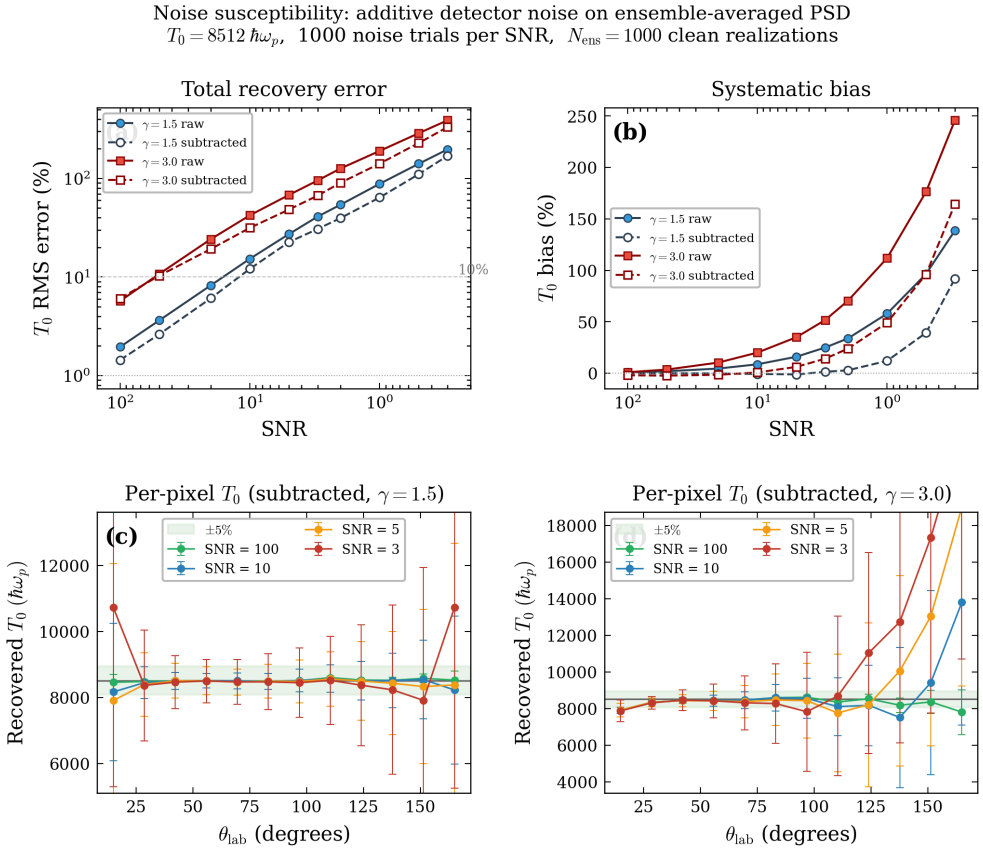


Figure 4: Noise susceptibility with additive detector noise: raw versus dark-subtracted recovery of T_0 as a function of signal-to-noise ratio.

4.2.7 Systematic uncertainties

Relative channel calibration. A multiplicative error α in relative E/B gain shifts $R_{\rm meas} = \alpha R$, giving $\delta\beta/\beta \approx \alpha - 1$ at low β; characterizable *in situ* with a known test signal or a source at known velocity.

Medium response function. Temperature extraction requires $\sigma(\omega)$; in the high-frequency regime only $T_0\nu$ is constrained by spectral shape, so σ must be characterized once (reflectivity, Thomson scattering, or Langmuir-probe analysis at rest). A fractional error $\delta\sigma/\sigma$ propagates as $\delta T_0/T_0 \approx \delta\sigma/\sigma$ *uniformly in angle*, leaving $\beta_{\rm EB}$ unchanged, so a misidentified σ is distinguishable from genuine anisotropy by the absence of angular trends.

Rest-frame calibration. The two-step protocol needs a $\beta = 0$ (or known low-drift) calibration; a residual $\beta_{\rm cal} \neq 0$ biases T_0 by $\sim \beta_{\rm cal}\cos\theta$ at leading order, requiring $\beta_{\rm cal} \lesssim 0.01$ for sub-percent recovery unless independently measured from the E–B ratio on the calibration data.

Departure from isotropy. A rest-frame anisotropy $\langle \delta E_y\, \delta B_x^* \rangle_{\rm rest} = \epsilon \langle |E_y|^2 \rangle$ (e.g. from beam-driven filamentation instabilities [27]) shifts the ratio to $R = 2\beta/(1+\beta^2) + \epsilon(1-\beta^2)^2/(1+\beta^2)^2 + O(\epsilon^2)$, biasing β by $\delta\beta \approx \epsilon/(2\gamma^2)$. A misidentified rest frame shows systematic angular trends in $T_0^{(\rm rec)}(\theta)$ rather than the flat profile, an internal diagnostic. Adversarial simulations (Fig. 5) confirm that anisotropy and conductivity mismatch produce distinct, separable signatures.

Shot-to-shot variation. Stochastic shot-to-shot fluctuations are mitigated by ensemble averaging provided the mean plasma state is stationary over the integration window.

Departure from equilibrium. Non-thermal features (beam instabilities, coherent emission) appear as excess power at specific angles or frequencies and degrade the fit to the smooth $T_0/D(\theta)$ profile, diagnosable from the reconstruction residuals.

4.2.8 Simulation algorithm

Each realization generates $N_{\rm mode}$ plane-wave modes in the comoving frame: frequency ω_n drawn uniformly from $[\omega_{\rm min}, \omega_{\rm max}]$; direction $\hat{k}_n$ isotropic ($\cos\theta_n$ uniform on $[-1,1]$, azimuth uniform); two transverse polarizations with complex Gaussian amplitudes $a_{j,n} = A_n(g_1 + i g_2)$, $g \sim \mathcal{N}(0,1)$ and envelope $A_n = \sqrt{T_0\, \sigma(\omega_n)/N_{\rm mode}}$ implementing the classical FDT; rest-frame fields $\mathbf{E}_n = a_{1,n}\hat{e}_{1,n} + a_{2,n}\hat{e}_{2,n}$, $\mathbf{B}_n = \hat{k}_n \times \mathbf{E}_n$. Modes are boosted along $\hat{z}$,

$$E'_{y,n} = \gamma(E_{y,n} + \beta B_{x,n}), \qquad B'_{x,n} = \gamma(B_{x,n} + \beta E_{y,n}), \tag{9}$$

(with the remaining components transforming likewise), and the laboratory angle follows from aberration $\cos\theta_n^{\rm lab} = (\cos\theta_n^{\rm rest} + \beta)/(1 + \beta\cos\theta_n^{\rm rest})$. Modes are binned by laboratory angle into pixels; the y-channel pixel power is $W_i = \sum_{n\in i} |E'_{y,n}|^2$. The velocity estimator is the mode-sum

$$\hat{R} = \frac{\mathrm{Re}\sum_n E'_{y,n} B'^*_{x,n}}{\sum_n |E'_{y,n}|^2}, \qquad \beta_{\rm EB} = \frac{1 - \sqrt{1-\hat{R}^2}}{\hat{R}}. \tag{10}$$

The two-step temperature inversion forms $\bar{W}_{\rm lab}(\theta_i)/\bar{W}_{\rm rest}(\theta_i)$, defines the measured Doppler factor

$$D_i^{(\rm meas)} = \sqrt{\frac{P_{E_y}(\theta_i, \beta_{\rm EB})}{P_{E_y}(\theta_i, 0)} \frac{\bar{W}_{\rm rest}(\theta_i)}{\bar{W}_{\rm lab}(\theta_i)}}, \tag{11}$$

and returns $T_{\rm lab}(\theta_i) = T_0/D_i^{(\rm meas)}$ and $T_0^{(\rm rec)}(\theta_i) = D_i\, T_{\rm lab}(\theta_i)$ with $D_i = \gamma_{\rm EB}(1 - \beta_{\rm EB}\cos\theta_i)$. The azimuth-averaged polarization factor $P_{E_y}(\theta,\beta)$ is computed numerically with $N_\phi = 300$ samples (convergence better than 0.1%); in the rest frame $P_{E_y}(\theta,0) = (1+\cos^2\theta)/2$. Additive noise is drawn as $W_i^{\rm noisy} = \bar{W}_{{\rm lab},i} + P_{\rm noise}\,\eta_i$ with $\eta_i \sim \mathrm{Exp}(1)$, dark subtraction removing the mean floor.

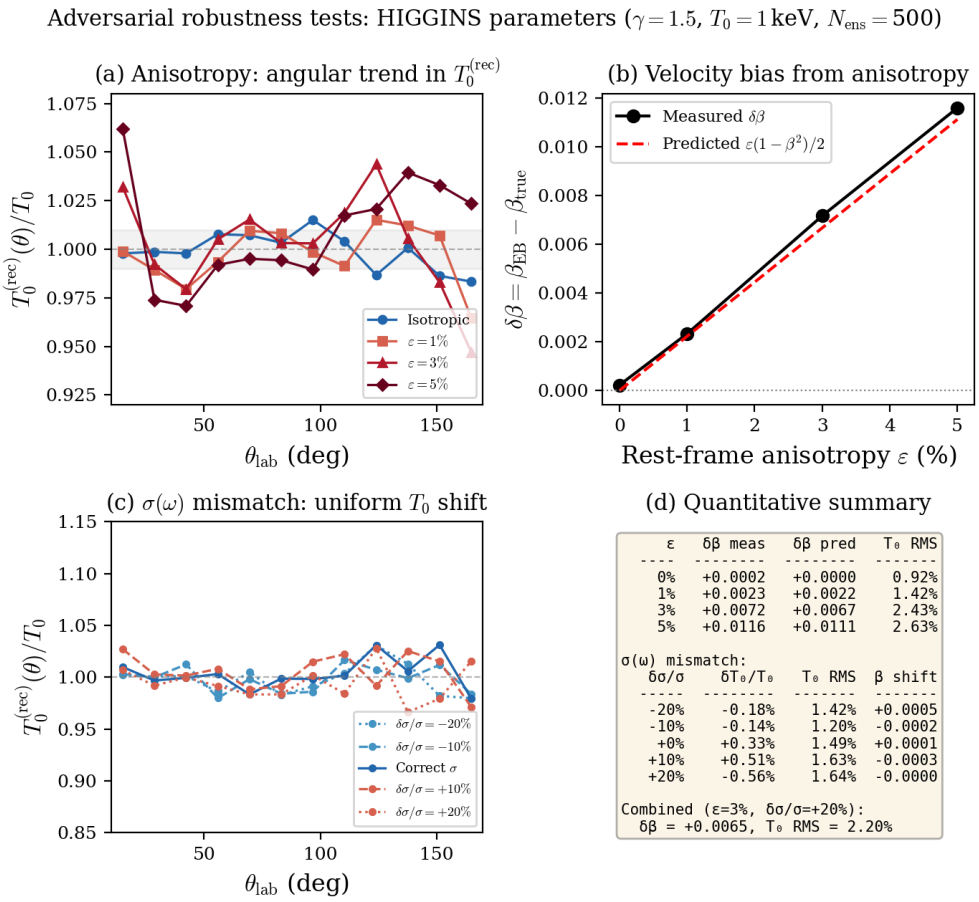


Figure 5: Adversarial robustness at HIGGINS parameters: injected rest-frame anisotropy biases β_{EB} and induces angular trends in $T_0^{(\mathrm{rec})}(\theta)$, while conductivity mismatch shifts T_0 uniformly without affecting β_{EB}: two experimentally distinguishable failure modes.

4.2.9 Simulation parameters

Table 1: Parameters for the HIGGINS laser-plasma simulations.

Parameter	Symbol	Value
Electron density	n_e	$10^{19}\,\mathrm{cm}^{-3}$
Plasma frequency	ω_p	$1.78 \times 10^{14}\,\mathrm{rad/s}$ ($f_p \approx 28\,\mathrm{THz}$)
Electron temperature	T_0	$1\,\mathrm{keV}$
Collision frequency	ν/ω_p	0.05
Modes per realization	N_{mode}	4×10^4
Frequency range	ω	$[0.1,\ 13.0]\,\omega_p$
Detector pixels	N_{pix}	12
Angular coverage	θ	15°–165°
Pixel aperture	$\Delta\theta$	3.4°
Detector radius	R	$50\,\mathrm{cm}$
Lorentz factors	γ	$\{1.05, 1.1, 1.2, 1.5, 2, 3, 5, 10\}$
Calibration realizations	N_{cal}	10^3
Boosted realizations	N_{boost}	10^3
Azimuth samples	N_ϕ	300
Repetition rate		$1\,\mathrm{Hz}$

4.3 Use of generative AI

The author used a generative AI assistant (Claude, Anthropic) for LaTeX formatting, copy-editing, and structural revision of the manuscript, and to render figures from the author's own simulation code. All scientific content, derivations, results, and claims are the author's own, and the author takes full responsibility for them.

Data availability

The Monte-Carlo simulation code that generates all figures in this work is publicly available at `https://github.com/beastraban/Wolfson-Simulations/tree/main/em_spectroscopy` (MIT license), including the scripts and parameters used for the $T_{\mathrm{lab}}(\theta)$ reconstruction, the multi-γ validation, and the noise and adversarial-robustness studies. The study is theoretical and uses no experimental data; all quantitative results are reproducible from the released code.

References

[1] M. Planck, Ann. Phys. (Leipzig) **26**, 1 (1908).

[2] H. Ott, Z. Phys. **175**, 70 (1963).

[3] P. T. Landsberg, Nature **212**, 571 (1966).

[4] N. G. van Kampen, Phys. Rev. **173**, 295 (1968).

[5] W. Israel and J. M. Stewart, Ann. Phys. (N.Y.) **118**, 341 (1979).

[6] F. Becattini, Acta Phys. Pol. B **47**, 1819 (2016).

[7] L. Gavassino, Phys. Rev. X **12**, 041001 (2022).

[8] C. Farías, V. A. Pinto, and P. S. Moya, Sci. Rep. **7**, 17526 (2017).

[9] S. Pouryazdan and B. Vakili, Phys. Lett. A **590**, 131860 (2026).

[10] D. N. Zubarev, *Nonequilibrium Statistical Thermodynamics* (Consultants Bureau, New York, 1974).

[11] C. Cercignani and G. M. Kremer, *The Relativistic Boltzmann Equation: Theory and Applications* (Birkhäuser, Basel, 2002).

[12] J. I. Kapusta and C. Gale, *Finite-Temperature Field Theory: Principles and Applications* (Cambridge University Press, 2nd ed., 2006).

[13] M. Le Bellac, *Thermal Field Theory* (Cambridge University Press, 1996).

[14] W. Busza, K. Rajagopal, and W. van der Schee, Annu. Rev. Nucl. Part. Sci. **68**, 339 (2018).

[15] J. Sheffield, D. Froula, S. H. Glenzer, and N. C. Luhmann, *Plasma Scattering of Electromagnetic Radiation* (Academic Press, 2nd ed., 2011).

[16] I. H. Hutchinson, *Principles of Plasma Diagnostics* (Cambridge University Press, 2nd ed., 2002).

[17] G. B. Rybicki and A. P. Lightman, *Radiative Processes in Astrophysics* (Wiley, 1979).

[18] P. Kumar and B. Zhang, Phys. Rep. **561**, 1 (2015).

[19] H. B. Callen and T. A. Welton, Phys. Rev. **83**, 34 (1951).

[20] R. Kubo, Rep. Prog. Phys. **29**, 255 (1966).

[21] F. Jüttner, Ann. Phys. (Leipzig) **339**, 856 (1911).

[22] P. T. Landsberg and G. E. A. Matsas, Phys. Lett. A **223**, 401 (1996).

[23] J. B. Johnson, Phys. Rev. **32**, 97 (1928).

[24] H. Nyquist, Phys. Rev. **32**, 110 (1928).

[25] E. Kroupp *et al.*, Matter Radiat. Extremes **7**, 044401 (2022).

[26] K. Issautier, N. Meyer-Vernet, M. Moncuquet, S. Hoang, and D. J. McComas, J. Geophys. Res. **104**, 6691 (1999).

[27] C. Ruyer, L. Gremillet, D. Bénisti, and G. Bonnaud, Phys. Plasmas **20**, 112104 (2013); arXiv:1310.7721.

Funding

No external funding supported this work.

Author contributions

I.W. conceived the study, performed the derivations and simulations, and wrote the manuscript.

Competing interests

The author declares no competing interests.